Supporting Information for "Generation of Heterogeneous Pore-Space Images Using Improved Pyramid Wasserstein Generative Adversarial Networks"

Linqi Zhu[1,2,*], ***Branko Bijeljic***[1], ***Martin J. Blunt***[1]

[1]Department of Earth Science and Engineering, Imperial College London, SW7 2BP, London, United Kingdom
[2]Key Laboratory of Marine Geophysics and Georesource, Institute of Deep-sea Science and Engineering, Chinese Academy of Sciences, 572000, Sanya, China

Contents of this file

Introduction Here we show additional results. We begin with a more comprehensive introduction to the algorithm. Then, we showcase the formulae of two-point correlation function and mean relative error, also statistical regularities of five samples two-point correlation functions. Finally, we present the overall results of image generation for the five samples, including visualization and comparison of parameters.

1 Algorithm

1.1 Training Phase

The training phase of a Improved Pyramid Wasserstein Generative Adversarial Network (IPWGAN) involves the simultaneous training of two models: a generator (G) and a discriminator (D). The generator G learns to generate data that is similar to the training data, while the discriminator D learns to distinguish between real data and the data generated by G.

Algorithm 1 Training algorithm for IPWGAN

Require: Training data set X, number of epochs N, batchsize m
Ensure: Trained generator G and discriminator D
  for epoch $= 1, N$ **do**
    for each batch **do**
      Sample batch of m noise samples $\{z^{(1)}, \ldots, z^{(m)}\}$ from noise prior $p_z(z)$
      Sample batch of m examples $\{x^{(1)}, \ldots, x^{(m)}\}$ from data generating distribution $p_{\text{data}}(x)$
      Update the discriminator by ascending its stochastic gradient:

$$\max_{\|D\|_L \leq 1} \frac{1}{m}\sum_{i=1}^{m} D(x^{(i)}) - \frac{1}{m}\sum_{i=1}^{m} D(G(z^{(i)}))$$
$$+ \lambda_1 \frac{1}{m}\sum_{i=1}^{m} \left(\|\nabla_{\hat{x}} D(\hat{x}^{(i)})\|_2 - 1\right)^2 + \lambda_2 \frac{1}{m}\sum_{i=1}^{m} \left(D(c^{(i)}) - D_{\text{FSM}}(c^{(i)}, s^{(i)})\right)^2$$

      Sample batch of m noise samples $\{z^{(1)}, \ldots, z^{(m)}\}$ from noise prior $p_z(z)$
      Update the generator by descending its stochastic gradient:

$$\min_{G} \frac{1}{m}\sum_{i=1}^{m} D(G(z^{(i)}))$$

    end for
  end for

1.2 Generation (Prediction) Phase

Once the IPWGAN has been trained, the generator model can be used to generate new data samples.

Algorithm 2 Data generation using a trained IPWGAN

Require: Trained generator G, number of samples n
Ensure: Generated data set Y

```
Initialize an empty data set Y
for i = 1, n do
    Sample noise z from noise prior p_z(z)
    Generate data y = G(z)
    Add y to the data set Y
end for
return Y
```

2 Formulae

The two-point correlation function, $S_2(r)$, is defined as follows:

$$S_2(r) = \frac{1}{V} \int_V \chi_\phi(\mathbf{x})\chi_\phi(\mathbf{x} + \mathbf{r})\, d\mathbf{x} \tag{S1}$$

where $\chi_\phi(\mathbf{x})$ is the characteristic function for the phase ϕ at location $\mathbf{x}$, $\mathbf{r}$ is the displacement vector between two points, and V is the volume over which the integration is performed.

The Mean Relative Error (MRE) is calculated as follows:

$$\text{Mean Relative Error (MRE)} = \frac{1}{N} \sum_{i=1}^{N} \frac{|V_{\text{true},i} - V_{\text{estimated},i}|}{|V_{\text{true},i}|} \tag{S2}$$

where $V_{\text{true},i}$ is the true value and $V_{\text{estimated},i}$ is the estimated value for the i^{th} data point, and N is the total number of data points.

The Mean Relative Error (MRE) for the two-point correlation function (TPCF) is calculated as follows:

$$\text{Mean Relative Error (MRE)} = \frac{1}{N} \sum_{i=1}^{N} \frac{|TPCF_{\text{true},i} - TPCF_{\text{estimated},i}|}{|TPCF_{\text{true},i}|} \tag{S3}$$

where $TPCF_{\text{true},i}$ and $TPCF_{\text{estimated},i}$ are the true and estimated TPCF values at the i^{th} distance point, respectively, and N is the total number of distance points.

3 Figures

Figures S1 - S3 show visualizations, two-point correlation functions and quantitative geometric and flow analysis of the characteristics of the five samples in the main text.

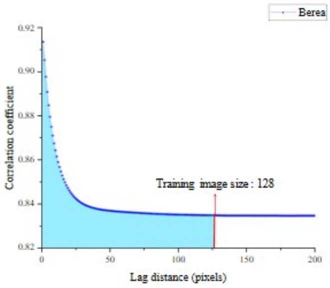

a. Berea sandstone

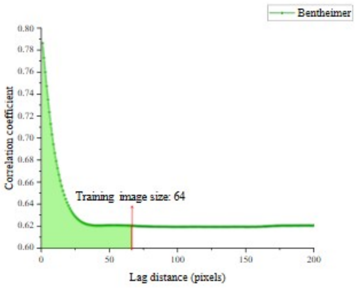

b. Bentheimer sandstone

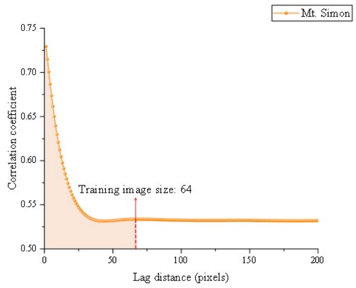

c. Mt. Simon sandstone

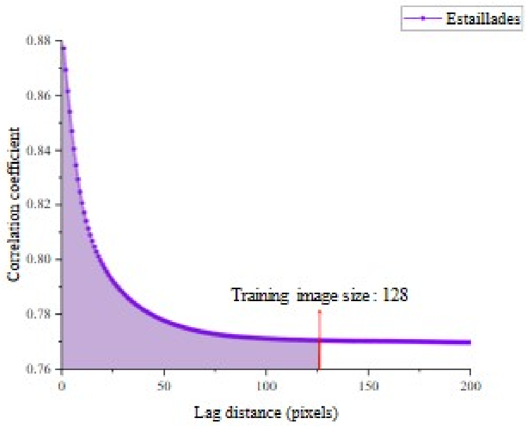

d. Estaillades carbonate

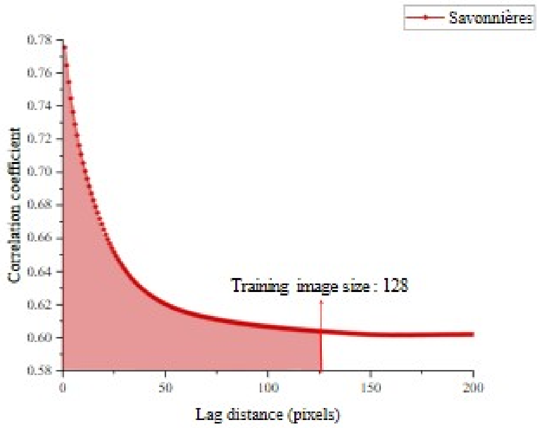

e. Savonnières carbonate

Figure S1: Two-point correlation functions for the five samples. For Bentheimer and Mt. Simon sandstones reach stability quikly while Berea sandstone, Estaillades carbonate, and Savonnières carbonate require a longer voxel distance to achieve stable function values. This reveals differences in heterogeneity, with Berea sandstone, Estaillades carbonate, and Savonnières carbonate display longer-range correlations. The results of the two-point correlation functions were used to select the size of the training images, which are evenly cut from the entire image. Considering the training speed of the GPU-based IPWGAN, for Bentheimer and Mt. Simon sandstones, a size of 64^3 is likely the optimal training image size. For Berea sandstone and Estaillades carbonate, 128^3 was chosen. Savonnières carbonate is a special case; strictly speaking, 256^3 would be its optimal training image size. However, training images of 256^3 demand excessive GPU memory, and even with a batch size reduced to 2, training may not be successful on a single NVIDIA Quadro RTX 5000. As this paper is more inclined towards exploring high-precision heterogeneous pore space image generation on a single GPU, the training image size for this image was chosen to be 128^3. As seen from the results in the main text, although sacrificing the size of the training image means that some of the longer-range connected pores are not perfectly restored, the recovery of multi-scale pore features is still very satisfactory. Under single GPU conditions, it is recommended to try using 256^3 images for training with the NVIDIA A100 (80GB) or even GPUs with larger memory.

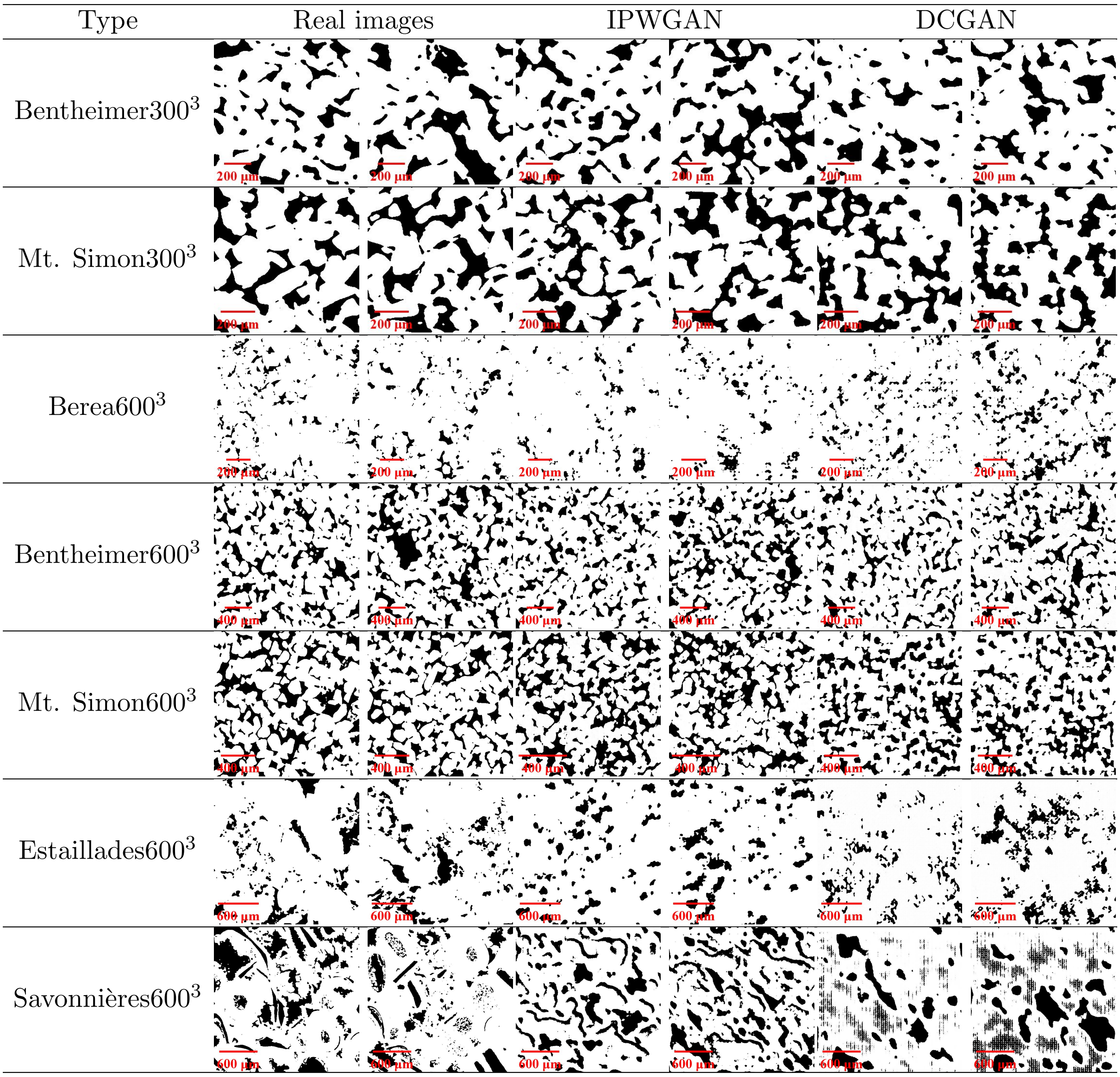

Figure S2: Visual comparison of two-dimensional cross-sections of three-dimensional images generated at different sizes, including results for Bentheimer and Mt. Simon of size 300^3, results for Berea, Bentheimer, Mt. Simon, Estaillades, and Savonnières of size 600^3

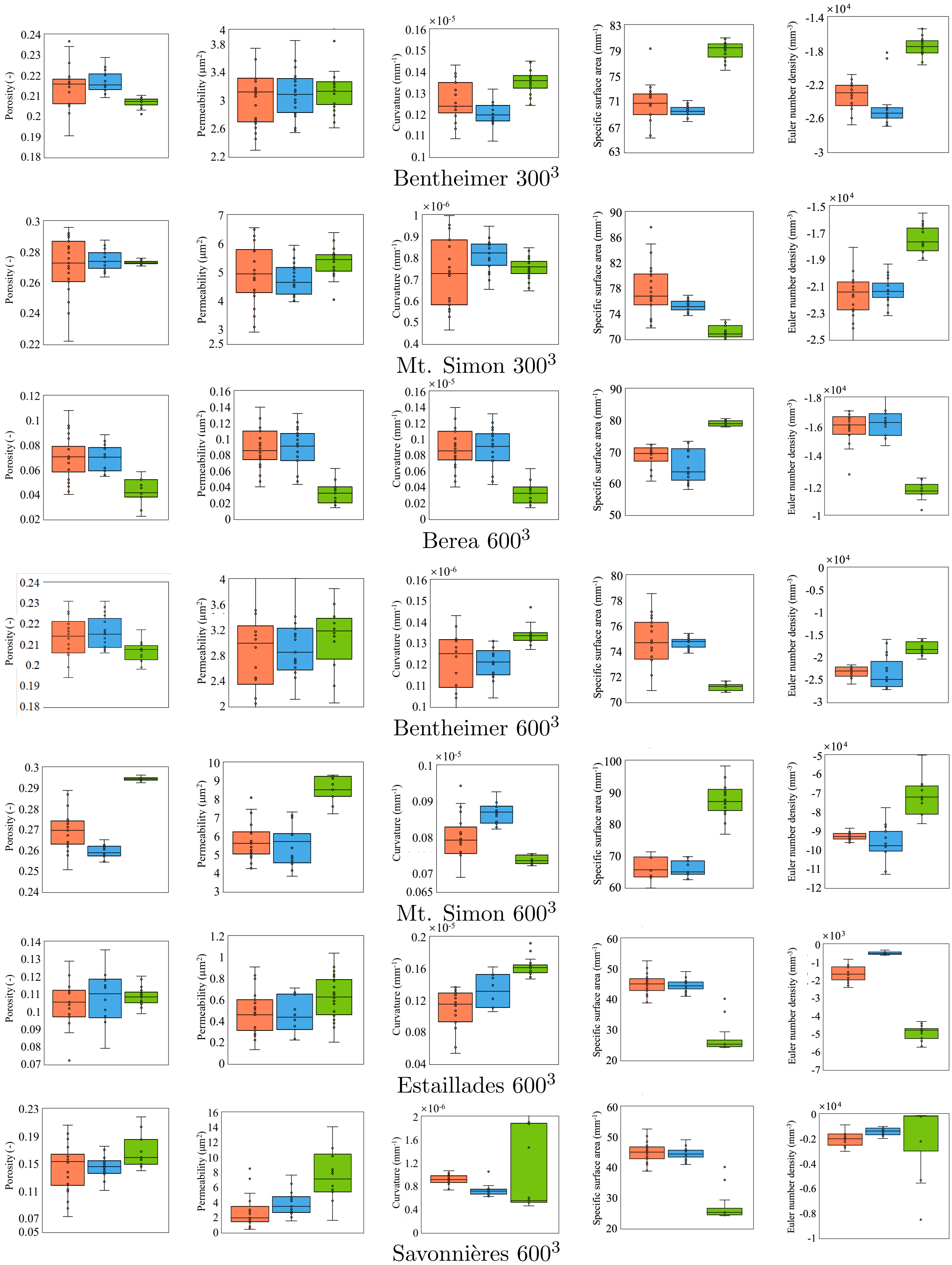

Figure S3: Parameter statistics for 300^3 and 600^3 images of five rock types: This section details the statistical outcomes for 300^3 images of five different rocks (excluding those covered in the main text) as well as the parameter results for all five samples of size 600^3. The statistics encompass connected porosity, absolute permeability, specific surface area, curvature, and characteristic per unit volume. In both cases, the 300^3 (Bentheimer and Mt. Simon) and the 600^3 for all five samples, the IPWGAN demonstrates superior performance.